Soft inertial microfluidics for high throughput separation of bacteria from human blood cells

Zhigang Wu[1*], Ben Willing[2], Joakim Bjerketorp[2], Janet K. Jansson[2,3] and Klas Hjort[1]

[1]Microsystem Technology, Department of Engineering Science, Uppsala University, Box 534, The Angstrom Laboratory, 751 21, Uppsala, Sweden

[2]Department of Microbiology, Swedish University of Agricultural Sciences, Box 7025, 750 07 Uppsala, Sweden

[3]Ecology Department, Earth Sciences Division, Lawrence Berkeley National Laboratory, Berkeley, CA, 94720

[*] To whom correspondence should be addressed (Zhigang.Wu@angstrom.uu.se)

Abstract

We developed a new approach to separate bacteria from human blood cells based on soft inertial force induced migration with flow defined curved and focused sample flow inside a microfluidic device. This approach relies on a combination of an asymmetrical sheath flow and proper channel geometry to generate a soft inertial force on the sample fluid in the curved and focused sample flow segment to deflect larger particles away while the smaller ones are kept on or near the original flow streamline. The curved and focused sample flow and inertial effect were visualized and verified using a fluorescent dye primed in the device. First the particle behaviour was studied in detail using 9.9 and 1.0 µm particles with a polymer-based prototype. The prototype device is compact with an active size of 3 mm^2. The soft inertial effect and deflection distance were proportional to the fluid Reynolds number (**Re**) and particle Reynolds number ($\mathbf{Re_p}$), respectively. We successfully demonstrated separation of bacteria (*Escherichia coli*) from human red blood cells at high cell concentrations (above 10^8 /mL), using a sample flow rate of up to 18 µL/min. This resulted in at least a 300-fold enrichment of bacteria at a wide range of flow rates with a controlled flow spreading. The separated cells were proven to be viable. Proteins from fractions before and after cell separation were analyzed by gel electrophoresis and staining to verify the removal of red blood cell proteins from the bacterial cell fraction. This novel microfluidic process is robust, reproducible, simple to perform, and has a high throughput compared to other cell sorting systems. Microfluidic systems based on these principles could easily be manufactured for clinical laboratory and biomedical applications.

1 Introduction

Microfluidics has gained significant advances in the past few years[1,2], especially for biological and medical applications[3]. One of the critical challenges in a microfluidic platform is the process for bio-particle selection, for example by filtration, fractionation, separation or sorting[3,4]. Initial efforts were focused on the miniaturization of fluorescence activated cell sorting (FACS) using microfluidic technology[5-10], or other active energy based switching approaches[11-16]. However, these systems are highly complex and resulting microfluidic platforms have been difficult to integrate. Techniques based on continuous fractionation by hydrodynamic interaction are attractive alternatives[17-24], due to their simple structure, robustness and potential high throughput, and because they are well suited to integrate into more complex microfluidic systems[25]. Until recently the maximum throughput has been in the range of 2,000 cells per min[25]. High throughput cell fractionation was very recently demonstrated using inertial force in an oscillating curved channel[22]. This approach originated from the tubular effect in circular channel observed by Segre and Silberberg[26] and theoretically explained and summarized by later studies; *e.g.* Saffman[27] and Matas *et al*[28]. With a flow rate of 1 mL/min and a throughput of about 50 million cells per min fractionation was demonstrated within a device area of ~2 cm^2. However at high flow rates, due to a "hard" inertial interaction and hence high shear stress near the walls, there is a large risk of stressing or even damaging sensitive cells without sheath flow protection [13]. Therefore, we suggest that at high flow rates a "soft" handling of cells should be made using sheath flow protection.

Although efforts have gone into separation of mammalian cells using microfluidics[3,4], there have been few investigations of this approach for microorganisms. None of the current systems have been developed for separation of bacteria from human cells. Due to the current interest in investigation of microorganisms living in association with humans; *i.e.* the human gut microbiome[29], new tools are required for efficient separation of bacterial cells from human cells. This is particularly problematic for biopsies, saliva, and other samples that have large amounts of human nucleic acids and proteins that can dominate subsequent "omics" applications, such as metagenomics or metaproteomics analyses, respectively.

Separation of bacteria from human cells in small sample volumes for omics applications presents several challenges. First, the method has to be rapid in order to prevent changes in mRNA or protein expression profiles. High throughput is thus required to separate the cells within a short time frame. Secondly, the method must work for small sample volumes with potentially low bacterial cell densities. For example biopsies are usually very small (approximately 3 mm^3) with a relatively low number of bacteria; *i.e.* 10^6-10^7 cells/biopsy. And finally the method must be able to separate a heterogeneous bacterial population, preferably in a viable state, from a heterogeneous mixture of human epithelial and blood cells. Methods currently available, such as fluorescence activated cell sorting (FACS) and others, are limited by speed, sample dilution, relatively large dead volumes and equipment access[30].

In this study we aimed to study a soft inertial force separation based on size differences for rapid and effective separation of bacterial cells from human blood cells. Red blood cells are particularly challenging to separate from bacteria because their disk shape results in a size close to that of bacteria in one dimension (2-3 µm) thus decreasing the effective size difference between the two cell types. Our hypothesis was that by using simple channel geometry with the help of acting and protecting sheath flow, a curved and focused sample flow segment would be formed to produce a soft inertial effect on the particles. Inertial interactions inside the curved and focused sample flow segment would result in deflection of larger particles (*i.e.* human cells) from the original streamline due to a subsequent soft inertial force while the smaller particles (*i.e.* bacteria) would remain close to the original streamline. To test this concept we designed delivery channels and collectors to specifically collect the bacterial cell fraction. We tested the design first by using differently sized synthetic particles and finally with a mixture of human blood cells and bacterial cells. Finally, sodium dodecyl sulfate polyacrylamide gel electrophoresis (SDS-PAGE) was used to demonstrate the removal of blood protein from the bacteria.

2 Theoretical background and the design principle

Various physical phenomena are competing in microfluidic devices[1]. Dimensionless numbers are often used to analyze these relations and their relative importance in various conditions.

The Reynolds number (**Re**) is defined as the ratio of inertial force to viscous force:

$$\mathrm{Re} = \frac{UD_h\rho_f}{\eta} = \frac{UD_h}{\upsilon} \qquad (1)$$

where U is the average velocity in the channel, ρ_f is the density of the fluid, η is the dynamic viscosity of the fluid, D_h is the hydraulic diameter of the channel, defined as $D_h = 2WH/(W+H)$ with channel width W and height H, and $\nu=\eta/\rho_f$, is the kinetic viscosity of the fluid inside the channel. When a particle is suspended in the fluid, naturally, it is influenced by the inertial and viscous forces from the fluid. The particle Reynolds number (**$\mathbf{Re_p}$**) can be defined as:

$$\mathrm{Re}_p = \mathrm{Re}\frac{a^2}{D_h^2} = \frac{Ua^2}{D_h\upsilon} \qquad (2)$$

where a is the diameter of the particle. For analysis of mass transport in the fluid, the particle behaviour can be observed through its Peclet number (**$\mathbf{Pe_p}$**), which describes the ratio between the mass transport due to convection and diffusion.

$$\mathrm{Pe}_\mathrm{p} = \frac{UD_h}{D} \qquad (3)$$

where D is the diffusion coefficient of the particle. For a sphere, it can be estimated by $D=k_BT/3\pi\eta a$, with the Boltzmann constant, k_B, and absolute temperature, T. For a particle in the accelerating flow its Stokes number (***St***) is used to describe how quickly the particle adjusts to the changes in the surrounding flow, which is defined as the ratio between the particle relaxation time (τ_r) to the characteristic time (τ_f) of the flow as below:

$$St = \frac{\tau_r}{\tau_f} = \frac{\rho_p a^2/18\mu}{D_h/U} = \frac{\beta a^2 U}{18\upsilon D_h} \qquad (4)$$

where $\beta=\rho_p/\rho_f$ and ρ_p is the particle density. A larger ***St*** means that the particle has a stronger preference to continue with its original velocity direction instead of following the fluid trajectory when the fluid is in accelerating motion.

In summary, the Reynolds number (**Re**) is used to describe the inertial effect of fluid flow in our application. The Peclet number (**Pe**) describes the mass transport contribution of molecules or particles. The particle Reynolds number ($\mathbf{Re_p}$) describes the inertial effect on a particle from a fluid. And the Stokes number (***St***) is useful to study trajectory mismatch between the particle and fluid, and the size separation effect although they are in the same flow condition, *e.g.* having the same **Re**.

2.1 Particle deflection

Reynolds number is often used to describe the flow state. Normally in microfluidics, due to a small **Re**, the inertial force can be ignored. However as **Re** increases the inertial force becomes apparent. For example, in some geometric configurations, such as a channel with a sudden turn or expansion, due to the wall restriction the momentous loss induced inertial force will produce an extra force (acceleration) on the fluid and subsequently lead to a secondary "Dean flow" inside the channel[1]. Considering the particles' suspension in the fluid, when $\mathbf{Re_p}$ is large enough the particles will have enough momentum to be able to escape the flow trajectory when the flow experiences a rapid change. Upon a rapid change in momentum, that is when ***St*** is large enough, a mismatch between the fluid and particles will appear. The subsequent force deflects the particles away from the fluid streamline and finally the particles escape from their original carrier fluid. With proper design and fluid control, some kinds of particles deflect from the original carrier fluid while others do not. For example, differences in behaviour demonstrated by differently sized particles can facilitate the separation of cells based on size.

Figure 1 illustrates an approach for continuous particle separation using the concept described above. A sample flow carrying the particle joins a stronger acting flow and they are introduced to a small channel at the same time. Due to the mismatching of the velocity, the particle flow will be focused and accelerated near the entrance. To avoid the direct interaction between the (bio)particle and the wall and subsequent large impact force on the (bio)particle, a very low flow rate sheath flow is also adopted to space the particle a bit out from the wall. Through this asymmetrical configuration, a curved and focused sample flow segment surrounded by sheath flows is formed for the particle flow. In Fig. 1a, from point 1 to point 3, the fluid element experiences momentum loss twice. From point 1 to 2, the fluid element loses momentum density $\Delta\rho u_1$, and the direction is towards the wall. From point 2 to 3, the fluid element loses momentum density $\Delta\rho u_2$, and the direction is far away from the original flow axis. The second momentum loss is more important since its introduced mismatch is not as restricted by the wall geometry as the first loss. Further, the mismatch can be amplified in a much broader acting flow.

Following Squires and Quake[1], and assuming the corner radius R and the turning time $\tau \sim R/U$, the fluid element momentum density loss leads to a corresponding inertial force density f_i. It can be estimated by:

$$f_i \sim \rho \frac{du}{dt} = \frac{\Delta(\rho u)_2}{\tau} \sim \rho \frac{U^2}{R} \qquad (5)$$

Assuming a sphere with the diameter of a, the inertial force F_i acting on the microsphere can be calculated by:

$$F_i = \rho \pi a^3 U / 6R \qquad (6)$$

This force leads the particle to deflect from the original carrier fluid axis. The migration will be balanced by Stokes drag,

$$F_s = 3\pi\eta a U_m \qquad (7)$$

where U_m is the particle migration velocity in the fluid. From equation (6), where the inertial force is proportional to a^3, and equation (7), where the balance force is proportional to a, a different behaviour with different size and finally separation can be expected. Further more, according to equation (4), if n is the size ratio of the large to the small particle, the size ratio proportionality of ***St*** is n^2. For example, in our application, the size of a red blood cell is estimated to be 6-8 µm and the size for a bacterial cell to be about 1-2 µm. The size ratio is thus somewhere between 3 and 8. Assuming the same density of the cells[†], the ratio of their ***St*** is in the range of 9 to 64. Therefore,, an amplified mismatch will increase the separation of the different cell types (Fig. 1b). With proper controlled fluid conditions, the large particles (green symbols, Fig. 1b; $\mathbf{Re_p}$ is big enough) are deflected away from the original carrier flow while the small particles ($\mathbf{Re_p}$ are small enough; follow the dashed line in Fig. 1b) and are kept inside. This results in fractionation of the two differently sized particles into two subgroups.

2.2 Device design

The device design includes (1) a curved and focused sample flow segment formation and (2) particle collection. For the curved and focused sample flow segment formation an acting flow was selected, which has a higher flow rate than the particle carrier fluid. Further, to obtain a turning effect the acting fluid was positioned vertically to the carrier fluid and joined in a straight channel (major channel). The flow rate of the acting fluid

[†] The densities of red blood cells and *E coli cells are only slightly different (red blood cell, 1.056-1.066 g/cm^3 and E. Coli 1.075-1.101 g/cm^3) as compared to their large differences in size; thus we consider it an adequate approximation to ignore the influence from density differences for our calculations.*

(Q_a) was much higher than the sample flow rate (Q), which was controlled by selecting syringe sizes using the same syringe pump. The acting channel also served as a sheath flow, which protected the direct interactions between the cells and the channel wall. However, it could only protect one side. Thus, another sheath flow was adapted to protect the opposite side. The influence of this new sheath flow was minimized by using a lower flow rate (Q_p). In the experiments, the acting flow rate was ten times the sample flow rate (Q_a=10Q) and the protecting flow rate was 2/5 or 1/5 of the sample flow rate (Q_p=2Q/5 or Q_p=Q/5).

The device schematics are shown in Fig. 1c. Three inlets including sample fluid, protecting and acting sheath flow converge in the major channel. The three collectors for small particles, large particles and waste are connected to the major channel downstream. Between the inlets and collectors, a control channel was designed, which is controlled separately with an extra pump. To simplify the tuning of cell separation a control channel, placed between the inlets and collectors and controlled with an extra pump, was designed to adapt and adjust to variations due to fabrication. By adding or subtracting fluid from the major flow, the spreading inside the major channel was shifted and finally the particle delivery could be tuned to its desired collectors[24].

3 Materials and methods

3.1 Materials and chemicals

For device fabrication, the silicone (polydimethylsiloxane, PDMS) Kit, Elastosil RT601A and B, were purchased from Wacker Chemie (München, Germany). SU-8 2050 with

developer was purchased from MicroChem, MA, USA and 4-inch silicon wafers from Wacker Chemie. Fluorescein disodium salt (Lancaster Synthesis, UK) was dissolved in deionized (DI) water and the pH was adjusted to 9 as recommended by the supplier. Sodium chloride, Alsever's solution, and phosphate buffered saline (PBS) buffer package were supplied from Sigma-Aldrich, St Louis, MO, USA. Tris(hydroxymethylamino)methane (TRIS), and 2-(4-morpholino)ethanesulfonic acid (MES), and for surface treatment hydroxypropylcellulose (HPC; 100 000 MW), were all purchased from Alfa Aesar, Karlsruhe, Germany. Suspensions of polystyrene latex microbeads with diameters of 1.0 µm (red fluorescent) and 1.9 or 9.9 µm (green fluorescent) were obtained from Duke Scientific, Palo Alto, CA, USA. For particle separation, the microbead stocks were diluted 1:5 in the DI water and 0.5% (v/v) Tween 20 (Alfa Aesar) was added to the suspensions to increase their stability and to help prevent clumping. Finally the particle suspensions were homogenized gently in an ultrasonic waterbath.

3.2 Device fabrication and fluidic control

The device was fabricated using standard soft lithography on PDMS and was bonded to the glass slide using plasma treatment[31]. To prevent cell adherence, the channel system was filled with 1.5% HPC dissolved in MES/TRIS buffer (80 mM/40 mM) after the plasma treatment. The device was then kept in a closed container with a high humidity environment in a refrigerator at 4ºC overnight. Before cell separation, the device was flushed with sterile PBS buffer[24]. For the experiments, three gastight syringes (Hamilton, Bonaduz, Switzerland) were filled with the fluids (sample and sheaths) and placed on an infusion syringe pump (PHD2000, Harvard apparatus, Boston, MA, USA). The tuning

flow was primed by a Univentor syringe pump (Univentor 864, Univentor, Malta). To maintain iso-electro-osmotic conditions, PBS was used for all fluids except sample solutions. The device was monitored by a CCD camera (Spot RL Mono, Diagnostic Instruments, MI, USA) attached on an inverted fluorescent microscope (Nikon TE2000-U, Tokyo, Japan).

3.3 Data acquisition and analysis

For tuning the separation, the microscope was operated in phase contrast mode to optimize cell contrast. For fluorescent particle separation and fluorescent dye visualization, a blue-green fluorescent attachment (Nikon B-2A, Excitation 450-490 nm, Emission 520 nm) was used while for the non-fluorescent particles phase contrast mode was used. In both cases, a 20× objective (NA 0.45) was used for observation. The particles' trajectories were recorded by the CCD camera for later study. After recording the images into a computer, the concentration profiles were evaluated using a self-developed program written in MATLAB (2007b, MathWorks, Natick, MA, USA) as described previously[32]. Subsequently, a path with the known position across the channel was evaluated. The position across the channel was normalized against the channel width, while the measured pixel intensity was normalized against the maximum and minimum intensities in the place where the fluids met. The corresponding width or distance was measured using the obtained profile. The fluorescent width near the entrance (w) was measured as the distance from the maximum to the position where the intensity becomes half (in acting flow). The reason for this distinction was that the protecting sheath was very thin and close to the channel, which made it difficult to measure the wall or half intensity of the fluorescent dye. For the measurement of the small particle dispersion, the

distance was measured from the position where the intensity became half in protecting sheath flow to the position where the intensity became half in acting flow.

3.4 Cell preparation and protein determination

Human blood was collected with a vacutainer tube (BD, Franklin Lakes, NJ, USA) from a healthy volunteer and kept in Alsever's solution at a ratio of 1:1 at 4ºC. The above blood solution (~$2.5x10^6$ red blood cells and $5x10^3$ white blood cells per µL) was then diluted with a cultured *E. coli* suspension (7.2 log colony forming units (cfu) per mL) at a ratio of 1:5 or 1:10 (v:v). The blood cell counts were determined by direct microscopic counting in a Bürker cell counting chamber (Fisher Scientific, Pittsburgh, PA, USA).

To demonstrate the removal of blood proteins from bacteria, SDS page protein gels were run on samples taken before and after separation. Briefly, the cell suspensions were centrifuged at 13,000 g for 5 min and the supernatant was removed. Cell pellets were suspended in 25 µL of phosphate buffered saline (PBS) and diluted in protein loading buffer (1:1) heated at 99ºC for 6 min. then loaded on an 8-25% PhastGel, run on a PhastSystem Separation unit (GE Healthcare Bio-Sciences). Coomassie blue (Pierce, Rockford, IL) was used to stain all proteins separated on the gel. The protein banding patterns of cell mixtures were compared to those of blood and pure bacterial cultures prior to the separation process.

4 Results and discussion

4.1 Fluorescent visualization

Fluorescent dye was used for visualization of fluid flow in the microfluidics device. One of the curved and focused sample flow segments is shown in the left panel of Fig. 1a. From our observation, the exact curvature of the sample flow varied with increasing Reynolds number (**Re**). The higher the **Re**, the stronger the influence of the acting flow on the sample flow shape. Although it is not easy to describe this influence quantitatively, we found there was a significant change in the width of sample fluid in the entrance of the major channel. We measured the fluorescent width (*w*) from a group of images taken with the same exposure and flow rate (**Re**), Fig. 2a. The *w* decreased slightly at first and then it increased rapidly along with the increasing **Re**. Normally, the dye diffusion coefficient is constant with the same concentration although we do not know the exact value. Thus, **Re** is proportional to the Peclet number (**Pe**) and at low **Re**, **Pe** is small and the diffusion is dominant. This diffusion naturally makes a slightly wider fluorescent width. With the larger **Pe**, the advection becomes more dominant. Although diffusion is still proceeding, the time decreases due to increased velocity of the fluid in the observed space resulting in a thinner fluorescent width. With the increasing **Re**, the inertial force eventually became strong enough to affect the (fluid) particle behaviour. A strong expansion appeared for the fluid and *w* became larger with the increased flow rate, as shown in Fig. 2a.

4.2 Particle observation

To observe the particle behaviour inside the device, 9.9 (green) and 1.0 (red) μm particles serving as large and small particles, respectively, were used to study the deflection of differently sized particles with the increasing flow rate inside the device. To maintain

consistency of the results, the flow rate ratio of the three fluids was kept constant as Q_a=10Q and Q_p=2Q/5 in all experiments with particles. To determine the extent of deflection of the large particles we measured the deflection distance (d_f) relative to the total channel width from the wall nearest the protecting sheath with increasing flow rate (**Re**), Fig. 2b. From the figure we can observe a clearly increasing curve with increasing Reynolds number of the large particles ($\mathbf{Re_{pl}}$)[‡]. Observing from $\mathbf{Re_{pl}}$ in the tested range, the larger particle behaviour is dominated by inertial force. For a clear separation of small particles the main concern is the extent of dispersion without being mixed with large particles. Thus, we measured the dispersion distance (d_d) for small particles relative to the total channel width, along the flow rate (i.e. the small particles' Peclet number $\mathbf{Pe_{ps}}$), Fig. 2c. Interestingly, the curve showed the same trend as in Fig. 2a. Finally, the peak distance (d_p) relative to the total channel width was measured along $\mathbf{Re_{pl}}$, Fig. 2c. As expected, a clear increasing trend was observed with increasing $\mathbf{Re_{pl}}$.

By observing the behaviour of the two kinds of particles as the flow rate increased, three stages were found (Figs. 2b and 2c). First, the particle deflection and dispersion were small. Then, the particle deflection and dispersion increased. Finally, the increase changed, being either slower or faster. Our application is limited at the highest flow rate since the particles will be restricted by the channel geometry. For small particles the dispersion could be explained by using the same discussion as above for the increasing fluorescent dye width. When the flow rate ($\mathbf{Pe_{ps}}$) is small, the diffusion is dominant. Later, with $\mathbf{Pe_{ps}}$ increasing, the advection is dominant. And finally, the inertial force induced

[‡] When $\mathbf{Re_{pl}}$ is 4.86 (Q=25µl/min), two peaks representing large particles appear, refer to Fig. 2e. Here, the larger one was used.

secondary flow is strong enough, which leads to a significant vertical dispersion along the major flow. A large particle, at the same **Re**, has a higher particle Reynolds number, $\mathbf{Re_{pl}}$, equation (2). Thus, the diffusion is not dominant even at the first stage for large particles. However, we observed that at first the large particles experienced a rapid increas of deflection as they moved into the inertial force dominant stage. Within this stage the deflection is first slowly increased and then more rapidly with increased $\mathbf{Re_{pl}}$. Finally the increase of deflection is slowed down.

By comparing Figures 2b and 2c, we found that the particle Reynolds number determined the particle behaviour. For the transaction from diffusion dominant to convection dominant, the critical Reynold number for particles ($\mathbf{Re_p}$) was approximately 0.002 while for the transition from convection dominant to inertial dominant, the critical $\mathbf{Re_p}$ was between 0.04 - 0.05.

Figure 2d shows the peak distance relative channel width along the $\mathbf{Re_p}$. Because the large particle deflection is far larger than that of the small one's, the curve trend is very similar to that of deflection of the larger particle. The results indicate that a higher $\mathbf{Re_p}$ is good for particle separation. However, they do not provide any hints about the potential risk for particles overlapping, which would result in mixing of the two kinds of particles at the interface. To study this issue, we studied the intensity of the fluorescent images at various flow rates. Figure 2e shows the normalized fluorescence intensity along the channel width. At a low flow rate, the particles were overlapping. With increasing flow rate, the overlap became smaller. The overlap disappeared at a moderate flow rate due to

stronger inertial interactions of the larger particles. Finally it returned back at higher flow rates since the stronger inertial interaction of small particles leads to very fast dispersal, which obscures the interface between large particles and small ones. Further, we plotted the ratio (d_f/d_d) of the large particles' deflection to small particles' dispersal distance along the larger particle Reynolds number (**Re_{pl}**). A clear separation was obtained at a high ratio when **Re_{pl}** was between 2 and 4, Fig. 2f.

4.3 Separation of bacteria from human blood cells

Due to the larger variation of bacterial and human cell sizes, as compared to that of the standard synthetic particles we used in the initial trials, the cell separation procedure required further modification. To assure clear separation of bacteria from red blood cells, we applied a control channel. This resulted in a better tuning of the separation of bacteria at a high sample flow rate, resulting in good separation at higher cell concentrations than previously reported[21,23]. The major contribution to separation in our device was deflection of larger cells. Thus, our bacterial cell separation was not as sensitive to cell-cell interactions as it would have been if using rotation induced migrational separation[23,26,27].

Figure 3 shows one example of the cell counts before and after separation at a sample flow rate of 15 µL/min with 10× dilution of a mixed red blood cell and bacterial cell sample. Using a Bürker cell counting chamber, we showed the relative fraction ratio of the cells before and after separation. The Bürker chamber has a constant depth of 100 µm, and known grid size, e.g. the smallest distance between the two lines in Fig. 3 is 25 µm. Therefore, the cell number concentration (number/volume) can be obtained by manually

counting under a microscope. In our experiment, it was used to obtain the information on cell fractionations and their ratios before and after separation. Figure 3 (a) showed the sample cells before separation. Some of the cells looked brighter than others (both blood cells and *E. coli* cells), presumably due to differences in their physiological status. After separation, only a few of the red blood cells could be found in the *E. coli* cell fraction while there were some more *E. coli* in the fractions of the red blood cells and very few cells in the waste, Fig. (b)-(d). In this example, the purity (the ratio between the number of recovered target cells to the total number of recovered cells) of bacteria was 99.87% at a high throughput of 57,400 cells per second and with a separation recovery of 62%. Further using the same sample, the cell separations were carried out at sample flow rates between 2 and 18 µL/min. Cell counts indicated that the *E. coli* cells were enriched at least 300 times. The results are summarized in Table 1.

Due to the relatively small size of red blood cells, the same particle Reynolds number will be reached by them at a higher flow rate than for most other human cell types. With a flow rate of 18 µL/min we still achieved good separation of the different cell types, which is higher than most of the previously reported cell separation rates[25]. The average velocity in the channel was about 1.6 m/s, which was not damaging to the bacteria as indicated by their ability to grow on culture medium after separation. At this flow rate, 7.07 log cfu of *E. coli* were recovered in the small particle fraction after separation from the original sample containing 7.24 log cfu, and the total cell survivability was greater than 95 %.

The protein banding pattern (Fig. 4) from the different cell fractions (cells from Fig. 3) demonstrates removal of blood cell proteins to such a degree that no contribution of proteins from blood cells were visible, thus demonstrating that the method resulted in efficient separation of bacteria from human red blood cells. As shown in Fig. 3, some of the *E. coli* cells were lost in the red blood cell fraction and waste. Similarly, the protein bands representative of the bacterial cells were seen in the banding pattern from the red blood cell fraction (Fig. 4 E), albeit at a lower signal intensity compared to that from the pure bacterial culture or the separated *E. coli* cell fraction (Fig. 4, A and D). Even so, it does not affect our major target to study the protein from bacteria; since the originally dominating human proteins were efficiently removed from the bacteria. This method makes it possible for further investigation of the microorganisms living in association with humans in molecular level.

For this separation method, one issue that needs to be considered before separation is that one has to decide whether to prioritize purity of the bacterial fraction, the number of bacteria collected (throughput), or the percentage of bacteria that are collected (recovery). Therefore, achieving higher bacterial cell recovery could be at the cost of increasing cross contamination and/or decreasing throughput.

5 Conclusions

The use of soft inertial force is proposed for a high throughput separation of bacterial cells from human red blood cells based on size differences. Our results indicate that the curved and focused sample flow segment plays a very important role in the separation

process and that the particle Reynolds number is a critical parameter for cell separation. Fabricated in polymer, the device shows promise as a cost-effective way to provide highly enriched viable bacterial cells from human blood with simple operation and robust performance.

Acknowledgments

The authors thank Dr. Sara Thorslund for assistance with cell preparations. This work is partly funded by the Swedish Research Council for Environment, Agricultural Sciences and Spatial Planning, through the Uppsala Microbiomics Center (www.microbiomics.se), and partly by the US Department of Energy (Contract No. DE-AC02-05CH11231) with Lawrence Berkeley National Laboratory.

References

1. T. M. Squires and S. R. Quake SR, *Rev Mod Phys*, 2005, **77**, 977.
2. G. M. Whitesides, *Nature,* 2006, **442**, 368.
3. J. El-Ali, P. K. Songer and K. F. Jensen, *Nature,* 2006, **442**:403.
4. P. S. Disttrich and A. Manz, *Nat. Rev. Drug Discov.,* 2006, **5**, 210.
5. A. Y. Fu, C. Spence, A. Scherer, F. H. Arnold and S. R. Quake, *Nat. Biotechnol.*, **1999**, 17, 1109.
6. D. Huh, A. H. Tkaczyk, J. H. Bahng, Y. Chang, H. H. Wei, J B Grotberg JB et. al., *J. Am. Chem. Soc*., 2003, **125** 14678.
7. P. S. Dittrich and P. Schwille, *Anal. Chem.*, 2003, **75**, 5767.

8. J. Kruger, K. Singh, A. O'Neil, C. Jackson, A. Morrison and P. J. O'Brien, *J. Micromech. Microeng.*, 2002, **12**, 486.
9. A. Wolff, I. R. Perch-Nielsen, U. D. Larsen, P. Friis, G. Goranovic, C. R. Poulsen, J. P. Kutter and P Telleman, *Lab Chip*, 2003, **3**, 22.
10. L. M. Fu, R. J. Yang, C. H. Lin, Y. J. Pan and G. B. Lee, *Anal. Chim. Acta*, 2004, **507** 163.
11. M. P. MacDonald, G. C. Spalding and K. Dholakia, *Nature*, 2003, **426**, 421.
12. A. Nilsson, F Petersson, H Jönsson and T Laurell, *Lab Chip*, 2004, **4**, 131.
13. X. Hu, P. H. Bessette, J. Qian, C. D. Meinhart, P. S. Daugherty and H. T. Soh, *Proc. Nat. Acad. Sci. USA*, 2005, **102**, 15757.
14. J. Voldman, M. L. Gray, M. Toner and M. A. Schmidt, *Anal. Chem.*, 2002, **74**, 3984.
15. N. Pamme and C. Wilhelm, *Lab Chip*, 2006, **6**, 974.
16. Y. Kang, D. Li, S. A. Kalams and J. E. Eid, *Biomed. Microdevices*, 2008, **10**, 243.
17. L. R. Huang, E. C. Cox, J. C. Sturm, R. H. Austin and J. C. Sturm, *Science*, 2004, **304**, 987.
18. J. A, Davis, D. W. Inglis, K J. Morton, D. A. Lawrence, L. R. Huang, S. Y. Chou, J C. Sturm and R. H. Austin, *Proc. Nat. Acad. Sci. USA*, 2006, **103**, 14779.
19. M. Yamada, M. Nakashima and M. Seki, *Anal. Chem.*, 2004, **76**, 5465.
20. S. Choi, S. Song, C. Choi, and J. K. Park, *Lab Chip*, 2007, **7**, 1532.
21. M. Di Carlo, D. Irimia, R. G. Tompkins and M. Toner, *Proc. Nat. Acad. Sci. USA*, 2007, **104**, 18892.
22. D. Di Carlo, J. F. Edd, D. Irimia, R. G. Tompkins and M. Toner, *Anal. Chem.*, 2008, **80**, 2204.

23. M. Chabert and J.-L.Viovy, *Proc. Nat. Acad. Sci. USA*, 2008, **105**, 3191.

24. Z. G. Wu, K. Hjort, G. Wicher and Å. Fex Svenningsen, *Biomed. Microdevices*, 2008, **10**, 631.

25. N. Pamme, *Lab Chip*, 2007, **7**, 1644.

26. G. Segre and A. Silberberg, *Nature*, 1961, **189**, 209.

27. P. G. Saffman, *J. Fluid Mech.*, 1965, **22**, 385.

28. J . P. Matas, J. F. Morris and E. Guazelli, Oil Gas Sci. Technol., 2004, **59**, 59.

29. P.J. Turnbaugh, R.E. Ley, M. Hamady, C.M. Fraser-Liggett, R. Knight and J.I. Gordon, *Nature*, 2007, **449**,804.

30. M. M Wang et al., *Nat. Biotechnol.* 2005, **23**, 83

31. Y. Xia and G.M. Whitesides, *Annu. Rev. Mater. Sci.*, 1998, **28**, 153.

32. Z. G. Wu, N. T. Nguyen and X. Y. Huang, *J. Micromech. Microeng.*, 2004, 14, 604.

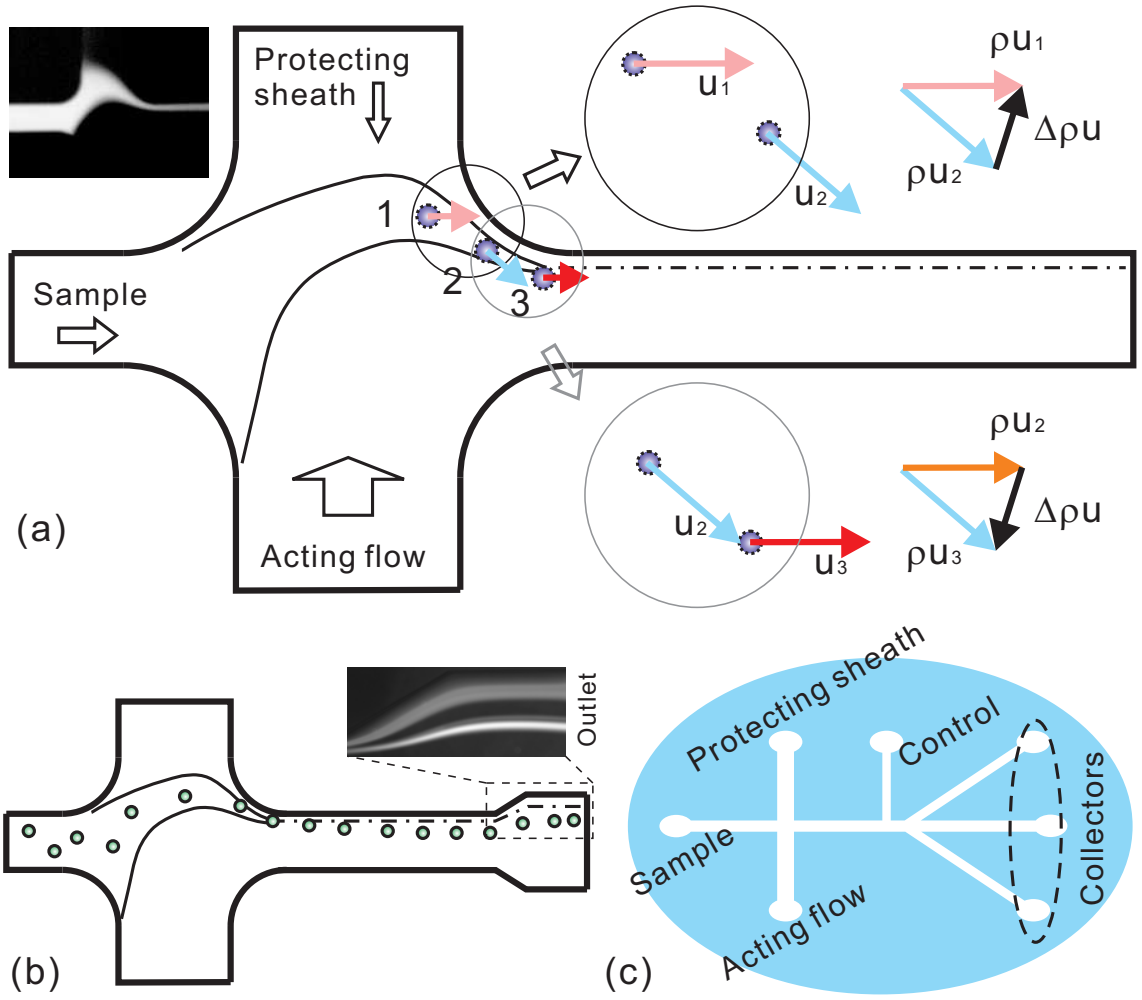

Fig. 1 The concept of soft inertial separation and schematics of device design: (a) the schematics of the formation of the curved and focused sample flow segment and particle momentous loss induced inertial force on fluid element (the top-left corner shows an example of fluorescent visualized curved and focused sample flow segment in the device); (b) the schematics of the particle separation in the device. The right corner shows an example of the larger particles (brilliant white curve near the center) deflecting from the ordinal sample flow (darker bright curve near the top) at the expanded outlet and (c) the schematics of the device design.

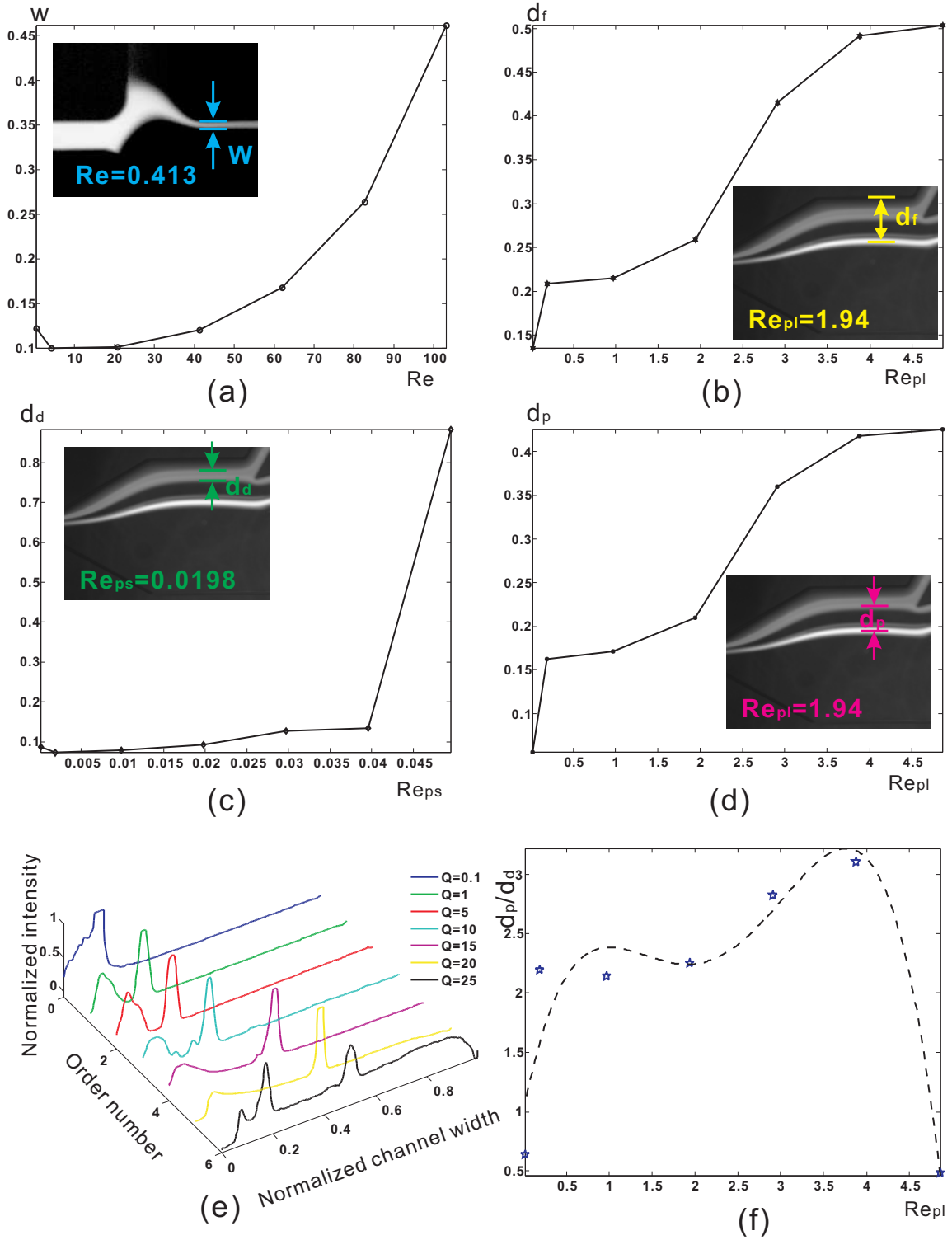

Fig. 2 The particle separation at various flow rates: (a) the relative sample width (w) at various **Re**; (b) the relative (large) particle deflection distance (d_f) from the wall at

various $\mathbf{Re_{pl}}$; (c) the relative (small) particle dispersion (d_d) at various $\mathbf{Re_{ps}}$; (d) the relative peak distance (d_p) between the larger and smaller particles at various $\mathbf{Re_{pl}}$; (e) the fluorescent intensity profile of particle trajectories at various flow rates (Q) and (f) the ratio (d_f / d_d) of large particle's deflection to small particle's dispersal distance along the larger particle Reynolds number ($\mathbf{Re_{pl}}$).

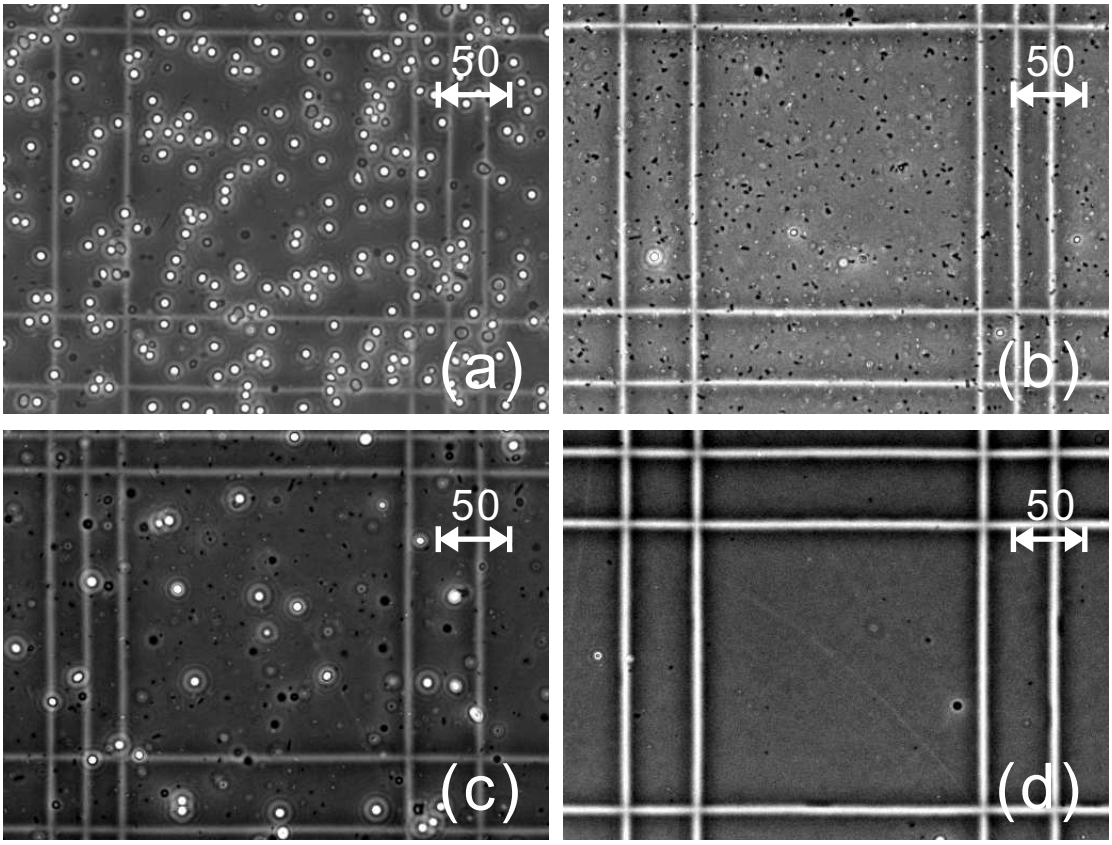

Fig. 3 Images of cells obtained by microscopy in a Bürker cell counting chamber: (a) the original sample diluted 10 times (the larger cells are red blood cells and the smaller cells are *E. coli*); (b) collected and separated *E. coli* cells after separation; (c) collected blood cells after separation and (d) the cells at the waste collector. The unit of the scale is in µm.

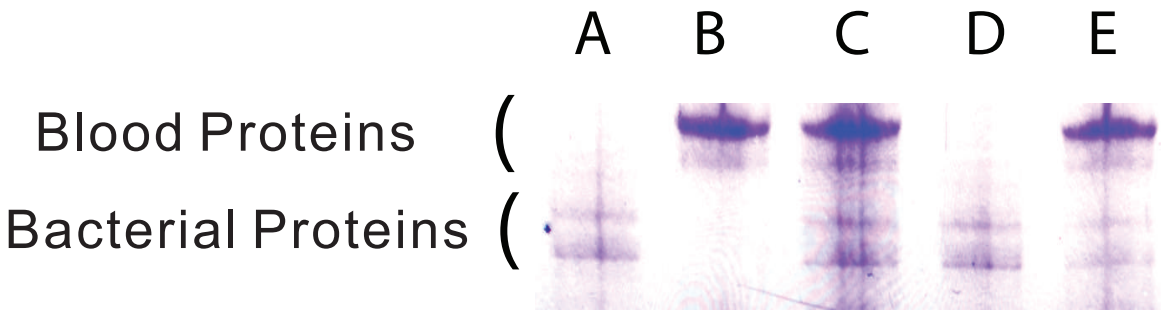

Fig. 4 Protein blot stained with Coomasie blue of: (A) *E. coli*; (B) blood cells; (C) original sample of combined blood and *E. coli* cells; (D) collected *E. coli* and (E) collected blood cells after separation (The blots C, D and E are from the same output as in Fig 3 (a), (b) and (c), respectively).

Table 1 Performance of separation of bacterial cells from blood cells

Flow rate (μL/min)	2	5	10	15	18
Purity (%)	99.88	99.78	99.86	99.87	99.71
Throughput (cells/s)	7653	19133	38267	57400	68880